Mechanism of Metal Intercalation under Graphene through Small Vacancy Defects

Yue Liu[a], Xiaojie Liu[a,b,], Cai-Zhuang Wang[c,d], Yong Han[c,d], James W. Evans[c,d], Ann Lii-Rosales[c,e,f], Michael C. Tringides[c,d] and Patricia A. Thiel[c,e]*

[a]Center for Quantum Sciences and School of Physics, Northeast Normal University, Changchun, 130117, China.

[b]Center for Advanced Optoelectronic Functional Materials Research, and Key Laboratory of UV Light-Emitting Materials and Technology of Ministry of Educations, Northeast Normal University, Changchun, 130024, China.

[c]Ames Laboratory, US Department of Energy and Iowa State University, Ames, Iowa 50011 USA

[d]Department of Physics and Astronomy, Iowa State University, Ames, Iowa 50011 USA

[e]Department of Chemistry, Iowa State University, Ames, Iowa 50011 USA

[f]Department of Chemistry, University of Colorado Boulder, Boulder, CO 80309 USA

KEYWORDS: defective graphene, first-principle calculations, detachment barrier, penetration barrier, intercalation

ABSTRACT: Metal intercalation under graphene has attracted extensive experimental and theoretical research, because of its capability to manipulate the electronic structure and properties of graphene. However, the pathways and mechanisms of intercalation are still not well understood. Here, we systematically investigate the intercalation process of metal atoms through graphene vacancies using first-principles calculations. We show that the energy barrier for metal atom penetration through the vacancies in graphene is small as long as the size of the vacancy is larger than a mono-vacancy. However, metal atoms are strongly bonded to the vacancy so that the detachment energy of a metal atom from the vacancy is extremely high. This inhibits the diffusion of the metal atom into the gallery beneath the surface to complete the intercalation process. On the other hand, our calculation results show that the detachment energy of a metal atom from a metal dimer at small vacancy defects is significantly reduced, making intercalation much easier. Therefore, the key step limiting the intercalation process is the detachment of the metal atoms from vacancy defects. This finding from our study provides useful insight into defect-assisted intercalation mechanism.

1.INTRODUCTION

Intercalation has been shown to be a very effective way to modify the electronic structure of graphene. It can be used to decouple the graphene layer from its substrate [1], to manipulate the graphene doping level [2,3], to control the magnetic properties [4,5], and to modify the electronic band structure of graphene [6-8], i.e., the position of Dirac point [9] as well as the shape of the Dirac cones [10]. In experiment, magnetic properties of transition metal intercalated graphene have been investigated for spintronic applications [4,5]. Alkali and the alkaline earth metals intercalation of graphene were also investigated for applications in energy storage [11] and superconductivity [12]. Moreover, novel properties of rare-earth metals intercalated graphene have also been reported [8,9,13].

Although intercalation in graphite and graphene on SiC or metal substrates have been extensively studied [1-13], the ability to perform intercalation in a controllable way, which is important for synthesis of desirable two-dimensional (2D) materials, is still a great challenge. Understanding the intercalation mechanism and pathway is critical for performing controllable intercalation. High temperature annealing is commonly used in experiment to facilitate the intercalation. While metal intercalation would take place even without pre-existing defects in graphene [14,15], pre-existing defects in graphene have been shown to play an important role in promoting the intercalation [16-21], where the defects can serve as the entrance of the intercalation channel. Although several possible mechanisms and pathways of intercalation, such as defect-assisted [22,23], intercalant-carbon atom exchange [14,15], penetration through line defects (e.g., grain boundaries, steps, wrinkles) [24], and passivation of strongly-binding unstable step edges configurations at defects with metal atoms [25], have been proposed, our understanding of intercalation process and mechanism so far are still very limited.

In this paper, we systematically investigate the intercalation pathways and mechanisms of transition and noble metals through a free-standing graphene with vacancy defects. In order to proceed the intercalation via the vacancy defects, penetration of the intercalant from the top side of the graphene to the opposite side is necessary. In the literature, such a penetration process and energy barriers have been calculated for several systems [22,25-28], and it is commonly assumed that the intercalation is governed by the penetration barriers. Here we show that the intercalation process is a complicated process even only through vacancy defects in graphene. In addition to penetration from the top level to the level below the vacancy, the process would also affected by the mobility of the intercalant away from the defects [25]. Experimentally, intercalation process involves metal atom adsorption and diffusion on the graphene surface, trapping by defects, switching from the top side to the bottom side of the graphene at the defects (we will refer to this process as penetration through the defects in the rest of the paper), and finally detachment from the defects to complete the intercalation underneath the graphene, as schematically shown in **Fig. 1**. We can see that the penetration of metal atom through the vacancy defects in graphene widely discussed in the literature is only one step among many other complex processes of the intercalation, and it is likely not the limiting factor determining the rate of the intercalation.

Taking Cu, Pt, Fe, Ru as prototype noble and transition metal intercalants and using first-principles calculations, we systematically study the energetics of adsorption and diffusion of the metal atoms on defect-free graphene, their trapping and penetration at small vacancy defects in graphene and subsequent detachment from the defects to identify the limiting factor for the metal intercalation under graphene with small vacancy defects. We show that the energy barrier for a metal atom to penetrate the graphene vacancy from one side to another side is not large as long as the size of the vacancy is larger than a mono-vacancy. However, the calculated results show that

the adsorption energy of Cu, Pt, Fe, Ru on the vacancy defects in graphene is very large, suggesting the metal atoms could be easily trapped by the defects and it is difficult to detach from the defects to complete the intercalation. Therefore, the detachment of the metal atom from the defects is the limiting factor for the intercalation. Then we propose a metal dimer assisted mechanism for metal intercalation through small vacancies. We show that the detachment energy for removing a metal atom from a metal dimer at the graphene defect is much reduced. At the same time, the penetration barrier from one side to another side for an intact metal dimer through either a mono-vacancy or di-vacancy in graphene is much smaller than detachment energy of a metal atom from the intact metal dimer at the defects. This interesting finding suggests that metal intercalation through graphene vacancy defects would take place through the metal dimer penetration at small (one or 2 missing carbon atoms) vacancy defects followed by the detachment of a metal atom from the metal dimer at the defects.

2.CALCULATION METHODS

The first-principles calculations are performed based on density functional theory (DFT) implemented in the Vienna Ab initio Simulation Package (VASP) [29-31]. The generalized gradient approximation (GGA) [32] in the Perdew-Burke-Ernzerhof (PBE) [33] formulation is used for exchange-correlation energy functional. Spin polarization and dipole moment correction are also included. PBE functional with spin polarization and dipole moment corrections has been widely used for accurate energetic calculation of graphene-based systems. To account for the electron-core interaction, the projector-augmented-wave (PAW) [30,31] method is adopted. For carbon atoms, $2s^2 2p^2$ electrons are considered to be valence electron configurations explicitly. $3d^{10}4p^1$, $5d^9 6s^1$, $3d^7 4s^1$ and $4d^7 5s^1$ electrons for Cu, Pt, Fe, Ru are treated as valence electrons in the calculations. The electronic wave functions are expanded in a plane-wave basis set using a kinetic energy cutoff

of 400 eV. In the geometry optimization, the atoms are allowed to relax until forces on each atom are smaller than 0.01eV/Å. The supercell dimensions are kept fixed during the relaxation. The energy convergence criteria is set to be 10^{-4} eV.

The primitive cell of graphene is a parallelogram with two carbon atoms. The lattice constant obtained from our calculation is 2.46 Å, which agrees well with the experimental value. The metal atom on defective graphene (i.e., 1~6 carbon vacancies named as V1~V6) system is modeled by having a metal atom in a 6×6 graphene supercell with periodic boundary conditions. A vacuum region of 15 Å is used in the z direction to avoid the interaction between graphene sheet and its periodic replicas. $4\times4\times1$ K-points sampling with the Monkhorst-Pack scheme is used for structural relaxations.

In order to obtain the energy barriers, such as the diffusion barriers and the penetration barriers, the climbing image nudged elastic band (CNEB) method [34] is performed to estimate the various energy barriers. The possible diffusion paths are assessed with CNEB and barriers are defined as the energy difference between the initial configuration and the maximum-energy configuration along the diffusion paths.

3. RESULTS AND DISCUSSIONS

3.1 Limiting factor for metal atom intercalation through small vacancy in graphene

As we mentioned in the introduction section and schematically shown in **Fig. 1**, the intercalation process is a complicated process, which involves metal atom adsorption and diffusion on graphene surface (**Fig. 1** (a)), trapping and penetration at the vacancy defect (**Fig. 1** (b)), and finally detachment from the defects to proceed the intercalation (**Fig. 1** (c)). We can see that the penetration of metal atom through the vacancy defects on graphene from one side to another side

widely discussed in the literature is only one step among many complex processes of the intercalation, and it is likely not to be the limiting factor determining the intercalation rate. In order to identify the limiting factor for metal intercalation through vacancy defects in graphene, we systematically investigate the energetics of all other steps involved in a metal atom intercalation process in addition to the commonly discussed penetration process.

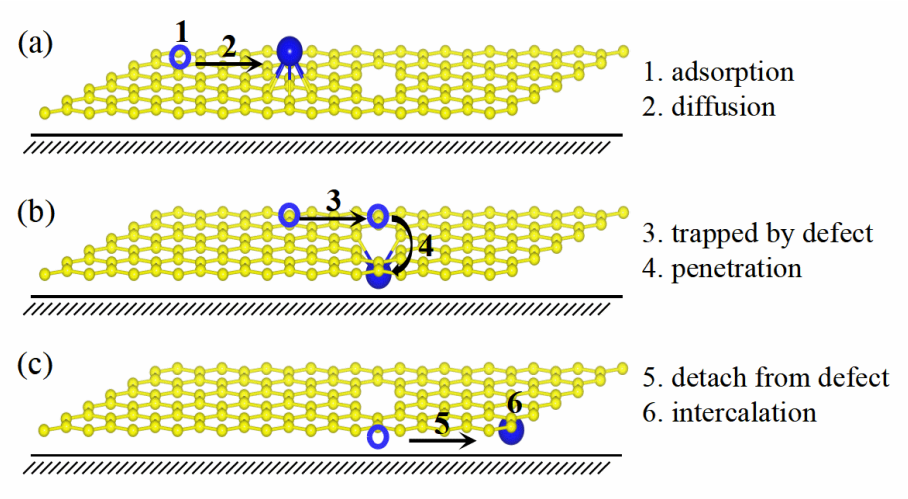

Figure 1. A schematic illustration of the process of a metal atom intercalation through a vacancy in graphene. (a) Metal atom adsorbs and diffuses on defective graphene. (b) Metal atom trapping penetrating at the vacancy defect in graphene. (c) Metal atom detaches from the graphene defect and diffuses along the graphene/substrate interface to complete the intercalation. Gold balls are C atoms, the open and solid blue balls are metal atoms, and the black horizontal line and slashes below the graphene indicate the substrate.

3.1.1 Adsorption and diffusion on pristine graphene

For comparison with adsorption and diffusion at the vacancies, we first examine the adsorption and diffusion of a metal atom on pristine graphene. Our previous studies [35,36] suggest that the energetic favorable adsorption site for Cu, Fe, Pt, and Ru atom on a free-standing graphene

is the top site (T-site), hexagonal-site (H-site), bond center site (B-site) and H-sites, respectively. The corresponding adsorption energies are 0.22 [35,36] ~0.5 [17] eV, 0.85 [35,36]~0.94 [19] eV, 1.56 [35,36] ~1.81 [21] eV and 1.89 [16]~1.97 [35,36] eV respectively for a Cu, Fe, Pt and Ru adatom. Therefore, the adsorption energy of Cu is the smallest, followed by that of Fe and Pt, and the adsorption energy of Ru is the largest. The adsorption strength indicates that interaction between Cu adatom and pristine graphene is weak while binding of Fe, Pt and Ru atom on graphene is stronger [16,17,19,21,35,36].

In addition, the diffusion barriers of Cu, Fe, Pt and Ru on a defect-free free-standing graphene surface are 0.004, 0.58, 0.19, and 0.62 eV [35,36], respectively. We note that for the metal adsorption and diffusion on multi-layer graphene, the values of the adsorption energy and diffusion barrier are slightly different [16,17,19-21,37], but the trend is very similar to the results on a free-standing graphene. The small diffusion barriers for the noble metal atom Cu and Pt indicate that Cu and Pt atom can diffuse almost freely on graphene surface. Larger diffusion barriers for the transition metal atom Fe and Ru make them more difficult to move on graphene surface.

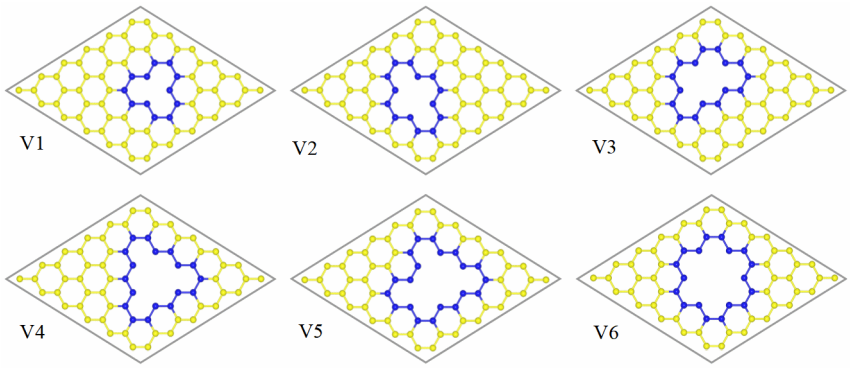

Figure 2. Structures of the of V1~V6 vacancy defects used in this calculation, where the number is the missing carbon atoms. Gold balls are C atoms away from the vacancies, blue balls are C atoms at edge of vacancies.

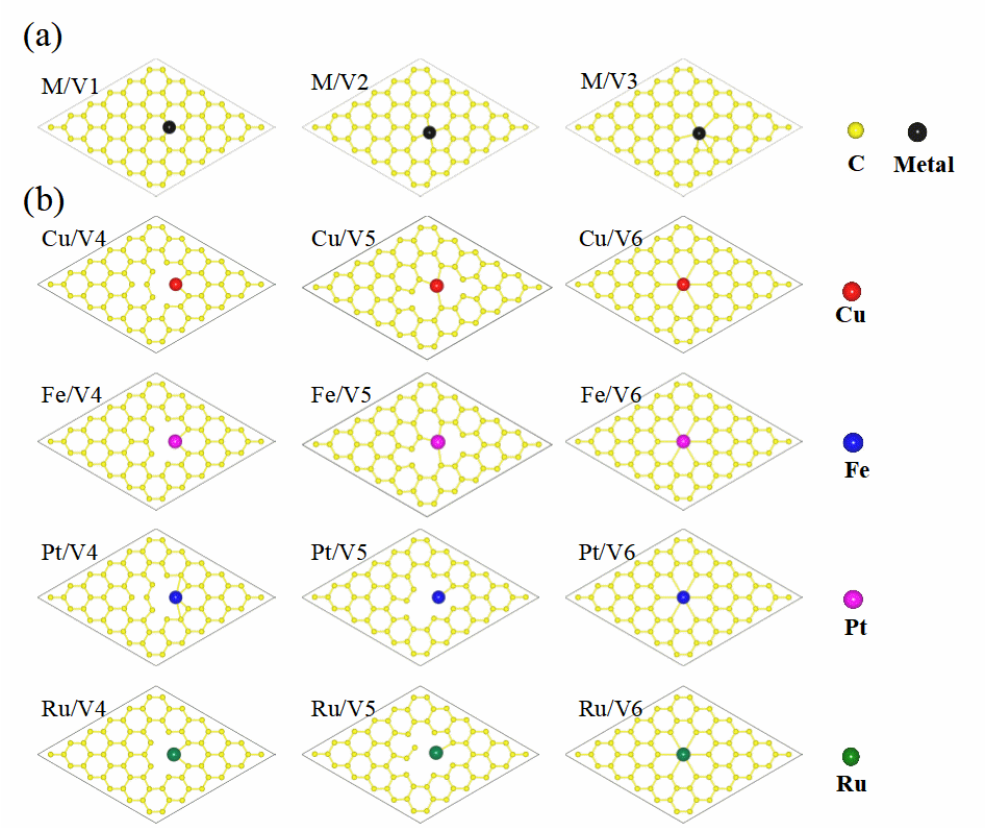

Figure 3. DFT optimized structures of single metal atom adsorption on V1~V6 vacancies in graphene.

3.1.2 Metal trapping at the vacancy defects in graphene

In order to evaluate the adsorption energy for the metal atom at the vacancy defects, we first construct and relax the low-energy configurations the vacancy holes V1~V6. These structures are shown in **Fig. 2**. The structures of V1~V3 are relatively simple and the metal atom can be initially placed at the center of the vacancy and then perform the structure optimization to determine the adsorption energy as one can see from **Fig. 3**(a). The structures for metal atom adsorption on V4-V6 are more complex. After structural optimization, we find the metal atoms are not always at the center of the vacancies for a metal atom adsorption on V4~V5, as shown in **Fig. 3**(b). We find that Cu, Fe, Pt and Ru atoms all prefer to attach to the edge of the V4~V5 vacancies. This result can

be understood as Cu, Fe, Pt or Ru atom tends to tightly bond with carbon atoms via metal-carbon bonds, thus leads to off center adsorption at the vacancies.

In order to evaluate the adsorption stability of the metals on V1~V6 defective graphene, adsorption energy is calculated by $E_a = E_M + E_{V_n} - E_{M/V_n}$. Here, E_{M/V_n} , E_M , E_{V_n} are the total energies of the metal atoms on V1~V6 defective graphene, metal atoms, and V1~V6 defective graphene, respectively. A more positive value of adsorption energy indicates a more energetically favorable adsorption.

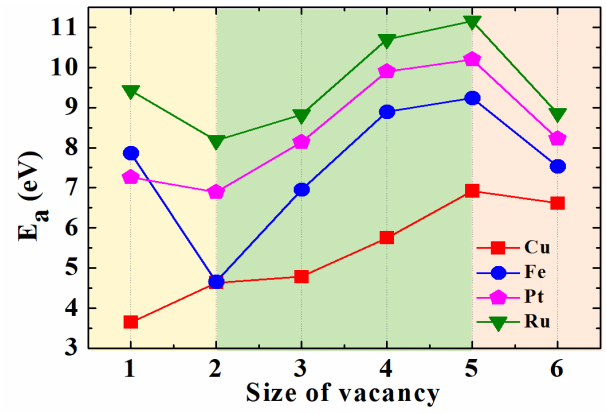

Figure 4. Adsorption energy of a metal atom (Cu, Fe, Pt, or Ru) on V1~V6 in graphene.

The adsorption energies of Cu, Fe, Pt, Ru on the graphene vacancies V1~V6 are plotted in **Fig. 4**. In order to gain more insights into the relationship between the adsorption energy and properties of the metal atoms as well as the structures of the defects, we also plot the area of defects, formation energy of defective graphene, averaged bond length of metal-carbon bonds as well as adsorption height as a function of the size of vacancy defects, which are shown in **Fig. 5**.

From **Fig. 4** we find that the trend of adsorption energies of Cu, Fe, Pt and Ru on the graphene vacancy defects follows Cu<Fe<Pt<Ru, except for Fe on V1 which will be discussed below. This trend is consistent with the trend in the covalent radius of the metal atoms. The covalent radius of

Cu, Fe, Pt, Ru is 1.32, 1.32, 1.36 and 1.46 Å, respectively. From the **Fig. 4** we also find that the adsorption energy increases as the size of the vacancy increases from V2 to V5, but decreases for V6. The adsorption energy also decreases from V1 to V2, except that for Cu adoption. Therefore, the adsorption energy can be divided into three groups, i.e., V1, V2~V5 and V6. When Fe and Pt atom adsorbed on V1, the adsorption energies are -7.86 and -7.26 eV, respectively. The strong Fe adsorption vs that of Pt are correlated the bond length of metal-carbon bonds. We find while the covalent radius of Fe and Pt atoms are not much different, the lengths of metal-carbon bonds are quite different for the two elements, 1.768 Å and 1.939 Å for Fe and Pt on V1, respectively. This result indicates that interaction between Fe atom and V1 is stronger than interaction between Pt atom and V1. It should be noted that the adsorption energy of Cu atom on V2 is comparable to that of Fe atom on V2, as one can see from **Fig. 4**. This is largely due to smaller bond length with the value of 1.894 Å for Cu-C bonds, while the bond length of Fe-C on V2 is 1.987 Å, as plotted in **Fig. 5**(a). The adsorption height of Cu and Fe on V2 defective graphene also exhibit similar trend which we can see from **Fig. 5**(b).

For Cu, Fe, Pt and Ru adsorbed on V2~V5, along with the increase in the area of defects (i.e., **Fig. 5**(c)) the adsorption energies gradually get large as shown in **Fig. 4**. This trend can be understood as the metal atom can form bonds with more than one carbon atom in larger vacancy where more dangling bonds exist with higher formation energy as one can see from **Fig. 5**(d). We note that the adsorption energies of all the 4 metal atoms in the current study on V6 become smaller than those on V5. The reduction of adsorption energy of metal on V6 suggests that weaker metal-carbon bonds are formed on V6 as can be seen from **Fig. 3**.

Comparison with the adsorption of Cu, Fe, Pt and Ru adsorption on pristine graphene, the adsorption energies of metal on defective graphene are significantly enhanced. The adsorption

energies of metals on V1~V6 suggest that the presence of defects on graphene surfaces is beneficial for increasing the interaction strength between the metal and carbon atom.

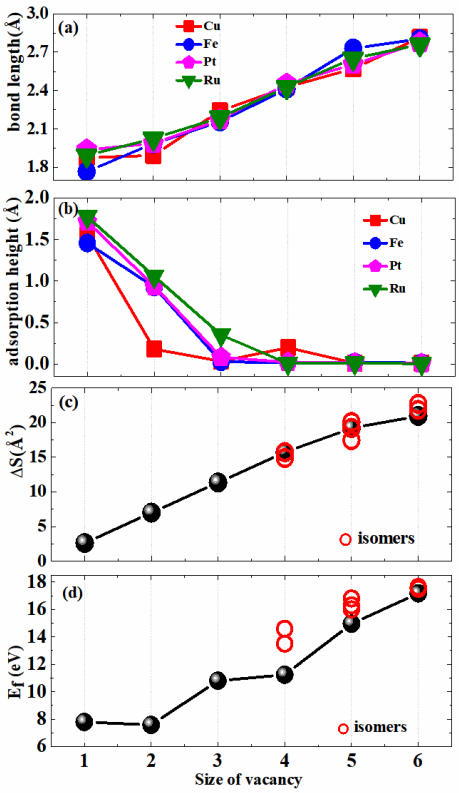

Figure 5. (a) Bond length of the metal-C bonds, (b) Adsorption height of the metal on V1~V6, (c) Area of the holes of the V1~V6, (d) Defect formation energy of the V1~V6 defined by $E_f=E_{total}-n\mu_c$, where μ_c is the chemical potential of carbon atom which is taken as the binding energy per carbon in perfect graphene from DFT calculation(-9.229eV), and n is the number of carbon atoms in the graphene with V1~V6 vacancies.

3.1.3 Energy barriers for metal atom penetrating the vacancies in graphene

It has been shown by experiment that pre-existing vacancy defects in graphene can facilitate the metal intercalation process [18]. Several theoretical calculations also showed that the energy barrier for metal atom penetration through vacancy defects is much lower than that through perfect

graphene [22]. Here we systematically calculate the energy barriers for Cu, Fe, Pt and Ru penetration through a free stranding graphene with vacancy defects of missing 1~6 carbon atoms (i.e., V1~V6).

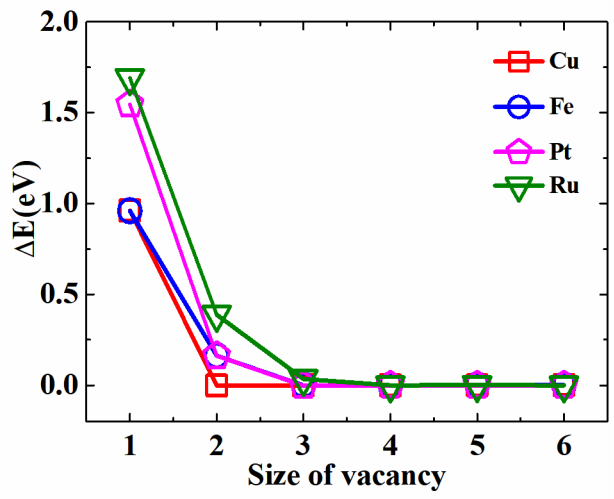

Figure 6. Energy barriers for single metal atom penetration through V1~V6 in graphene.

It has been reported that the energy barrier for the penetration depends on the size and electronic structure of the intercalant, and the conditions of the graphene, such as the nature and size of the defects in the graphene. For metal atom penetration through the vacancy defect in graphene, the penetration energy barrier is strongly correlated with the size of the metal atom and size of vacancy. Our calculated penetration barriers for Cu, Fe, Pt and Ru atoms through V1~V6 in graphene as function of the size of defects are plotted in **Fig. 6**. For Cu, Fe, Pt and Ru atoms on V1~V2, the penetration barriers follow Cu<Fe<Pt<Ru, which is the same as the trend of atomic radius. The penetration barriers for metal atoms on V3~V6 are close to zero, indicating that single atom penetration through the vacancies in graphene can take place almost spontaneously as long as the size of the vacancy is larger than V2.

Table 1. The adsorption energy (E_a, in eV) of single metal atom on V1~V2 in graphene and on pristine graphene; penetration barrier (ΔE_p, in eV) of a metal dimer through V1~V2 in graphene; detachment energy (ΔE_d, in eV) of a metal atom from V1 and V2 and from a metal dimer or a metal trimer on V1~V2 in graphene.

	Cu	Fe	Pt	Ru
E_a(V1)	3.64	7.86	7.26	9.43
E_a(V2)	4.63	4.66	6.90	8.19
Ea(V0)	0.22[35]	0.85[35]	1.56[35]	1.97[36]
ΔE_p(M2/V1)	0.38	0.30	0.34	0.03
ΔE_p(M2/V2)	0.28	0.16	0.21	0.15
ΔE_d(M/V1)	3.42	7.01	5.70	7.46
ΔE_d(M/V2)	4.41	3.81	5.34	6.21
E_a(M2/V1)	5.44	10.39	10.93	12.44
E_a(M2/V2)	6.36	9.82	10.14	11.97
E_a((M+M)/V1)	3.88	9.33	8.75	11.69
E_a((M+M)/V2)	5.08	7.78	8.40	10.46
ΔE_d(M2/V1)	1.56	1.06	2.18	0.75
ΔE_d(M2/V2)	1.28	2.04	1.74	1.51
E_a(M3/V1)	7.67	14.20	14.74	17.39
E_a(M3/V2)	8.48	13.34	13.62	16.52
E_a((M+M2)/V1)	5.70	11.84	12.44	14.71
E_a((M+M2)/V2)	6.59	11.20	11.66	14.29
ΔE_d(M3/V1)	1.97	2.36	2.30	2.68
ΔE_d(M3/V2)	1.89	2.14	1.96	2.23

3.1.4 Detachment of metal atom from the graphene defects

In the present calculation, we approximately estimate the detachment barrier as energy difference between metal atom adsorption on pristine graphene and at the graphene defect. We call this value as detachment energy.

Our calculated results for detachment energies of Cu, Fe, Pt and Ru atoms on V1 and V2 are listed in **Table 1**. The detachment energies are 3.42, 7.01, 5.70 and 7.46 eV respectively for Cu, Fe, Pt and Ru on V1 and 4.41, 3.81, 5.34, 6.21 eV respectively for Cu, Fe, Pt and Ru on V2. We would like to note that these values of detachment energies are calculated with a single layer free-standing graphene. For graphene on substrate, the detachment energies for the metal atoms to move away from the vacancy defect at the graphene/substrate interface would be different from the values given above since the metal atom also interacts with the substrate [38]. However, such difference should likely to be less than 1.0 eV since the interaction of the metal atom with the substrate could be similar when it is located below the vacancy or below the pristine graphene. Therefore, our calculation results of larger detachment energy indicate that it is very difficult for Cu, Fe, Pt and Ru atoms to escape from defects to proceed the intercalation into the graphene/substrate interface, although the penetration barriers are small when the size of the vacancy is larger than V1, as discussed above. Therefore, we can conclude the detachment energy for the metal atom from the vacancy defect is the limiting factor for the intercalation, not the penetration barrier through the vacancy as discussed widely in the literature. We note that in a recent paper [25], detachment of Cu atom from graphene step was also identified as the limiting factor for Cu intercalation through graphene steps.

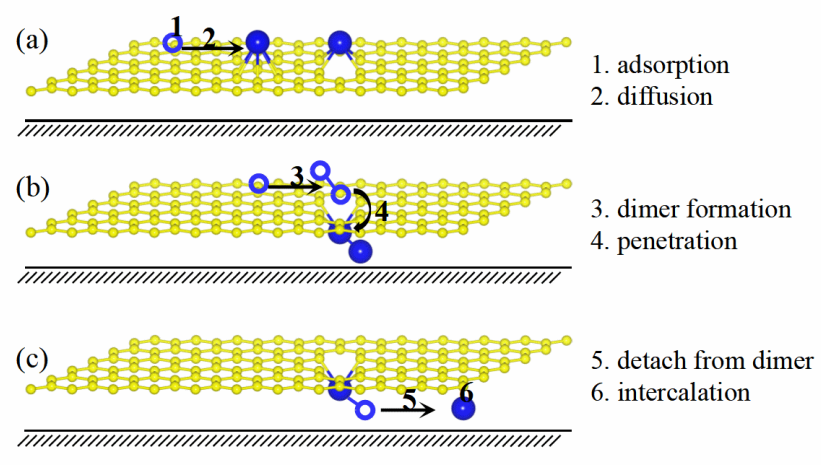

Figure 7. A schematic illustration of the metal dimer-assisted process for a metal atom intercalation through a vacancy in graphene. (a) Metal atom adsorbs and diffuses on the graphene with a pre-existing metal atom at the vacancy; (b) A metal dimer formation at the vacancy and penetration through the vacancy; (c) A metal atom detaches from the metal dimer and then diffuses along the graphene/substrate interface to complete the intercalation. Gold balls are C atoms, the open and solid are metal atoms, and the black horizontal line and slashes below the graphene indicate the substrate.

3.2 Mechanism of metal intercalation through small vacancies in graphene

Our calculations in the previous section indicate that the limiting factor for metal intercalation through small vacancy defects in graphene is the detachment energy of the metal atom from the defects. The large detachment energy limiting the intercalation is due to the strong metal-carbon chemical bond formed by the dangling bonds of carbon atoms at the vacancy defect. Therefore, precursors with pre-existing metal atoms at the vacancy defects to passivate the carbon dangling bonds are likely to help the intercalation of the later coming metal atom. Based on this conjecture, we calculate the adsorption energy for the metal atom to adsorb on the V1 and V2 defects with one pre-existing metal atom (we call these defects as M/V1 and M/V2). The intercalation process

for a metal atom through the M/V1 (or M/V2) defect is schematically shown in **Fig. 7**. A metal adatom on graphene surface is captured by the M/V1 (or M/V2) defect and form a metal dimer at the vacancy. We call the configuration of a metal dimer at the V1 or V2 vacancy as M2/V1 or M2/V2. Once the metal dimer is formed at the vacancy, it penetrates the vacancy and then one metal atom is detached from the metal dimer to complete the intercalation.

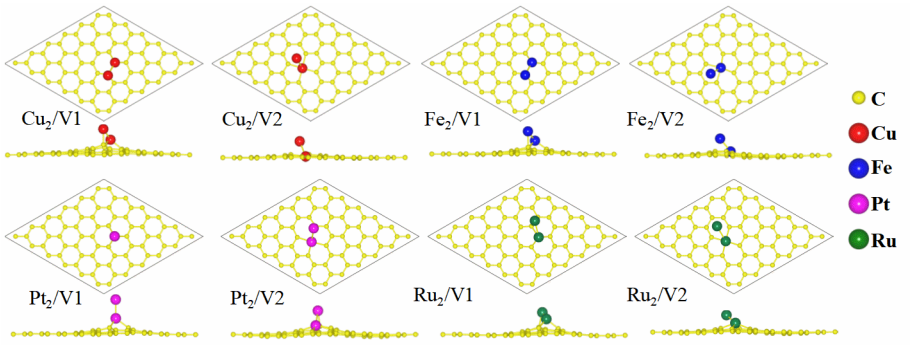

Figure 8. DFT optimized structures of the metal dimers on V1-V2 in graphene.

The detachment energies for the metal atom to escape from M/V1 and M/V2 are directly related to the corresponding adsorption energies of the metal atom on M/V1 and M/V2. Such adsorption energies are given in **Table 1**, which are significantly smaller than the adsorption energies for the metal on V1 and V2. The detachment energy of a metal atom from M/V1 or M/V2 defect configurations is then calculated by the difference between the adsorption energy for two metal atoms at the defect (see **Fig. 8**) and that of one metal atom at the defect while another metal atom on the graphene surface far away from the defects. The calculated detachment energies are also shown in **Table 1**. In order to check if the detachment barrier is different from the detachment energy calculated this way, CNEB calculations are carried out for Cu and Ru atom detaching from the metal dimer on V1 and V2. The detachment barriers are plotted in **Fig. 9**, which show that the detachment energy defined above is very similar to the detachment barrier from the CNEB calculation.

It is interesting to note that the detachment energies of a metal atom from the metal dimers at defects are reduced significantly. The detachment energies for one Cu, Fe, Pt and Ru atom from their dimers on V1 are reduced from 3.42, 7.01, 5.70 and 7.46 eV to 1.56, 1.06, 2.18 and 0.75 eV, respectively. The detachment energy of a metal atom from the metal dimers at V2 is also much lower than that from a single metal atom on V2 as one can see from **Table 1**. Based on these results, it is likely that a metal interaction of graphene can take place though the formation of metal dimer at the small vacancy defects as long as the penetration barrier for the metal dimer to switch from the top to bottom side of the graphene through the V1 and V2 defect is not larger than the detachment barrier.

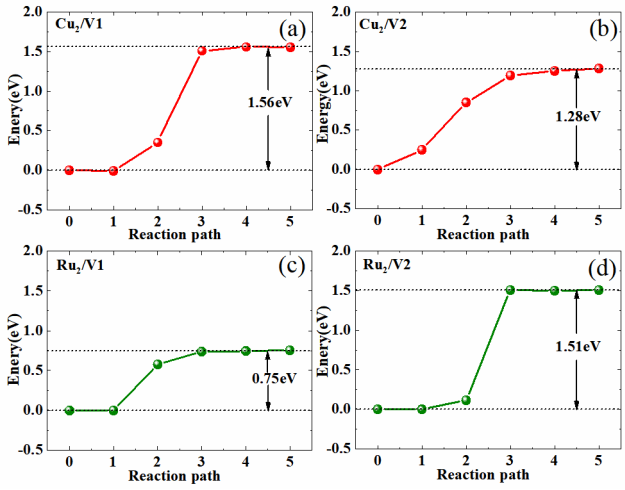

Figure 9. Energy for a Cu or Ru atom detaches from the corresponding metal dimer at V1 and V2 along detachment path determined by CNEB calculations.

In our present study, the energy barriers for the metal dimer to penetrate the V1 or V2 in graphene are calculated by pushing the top metal atom in the dimer along the line connecting this metal atom in the initial (i.e., M2 on top of graphene) and final (i.e., M2 underneath graphene) configurations of the dimer. At each point along the penetration pathway, the top metal atom is fixed while the other metal atom and surrounding carbon atoms are relaxed. The penetration

barriers calculated in this way for Cu, Fe, Pt and Ru dimers through V1 and V2 defects in graphene listed in Table 1.We can see that the energy barriers are 0.28, 0.16, 0.21 and 0.15 eV respectively for Cu, Fe, Pt and Ru dimer penetrating through V2 defective graphene, which are comparable to the penetration barriers of single Cu, Fe, Pt and Ru through V2 in graphene. We note that the energy barriers estimated in this way would be slightly higher than the actual penetration barriers, but they are sufficient to support our claim that penetration barrier for the metal dimer to switch from the top to bottom side of the graphene atom through V2 defect is much smaller than the detachment barrier and they are not the limiting factor for the intercalation.

Therefore, it is not difficult for metal dimer to penetrate through the defective graphene due to the small penetration barriers, and the main factor governing the intercalation is the detachment of a metal atom from the metal dimer at the vacancy defect. Since the detachment energy of a metal atom from such a dimer configuration is greatly reduced as compare to that from the bare vacancy, the probability for metal intercalation through the formation of a metal dimer at the small vacancy defect (i.e., V1 or V2) as an intermediate step would increase significantly at high annealing temperatures.

Moreover, in order to verify the detachment a metal atom from metal dimer at V1 and V2 is an optimum process, we also calculate detachment energy for a metal atom to detach from a metal trimer at V1 and V2 in graphene. The calculated detachment energies are 1.97 and 1.89 eV for Cu, 2.36 and 2.14 eV for Fe, 2.30 and 1.96 eV for Pt, 2.68 and 2.23 eV for Ru from the corresponding trimer at V1 and V2, respectively. The detachment barriers from the metal trimers are slightly higher than those from the metal dimers. **Fig. 10** shows the detachment energies of a metal atom from V1-V2, metal dimers at V1-V2 and metal trimer at V1-V2 in graphene. From the figure we can see that the detachment energy for a metal atom from the metal dimer is the lowest one,

followed by detachment from the metal trimers. Detachment of a metal atom from the bare vacancy is very hard.

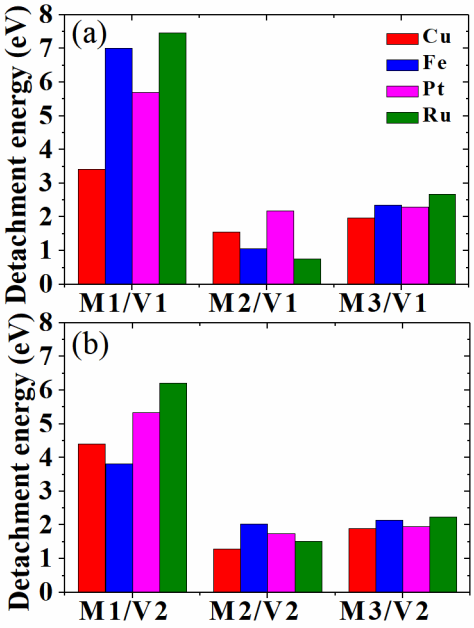

Figure 10. (a) Detachment energies of a metal atom from V1 (M1/V1), a metal dimer at V1 (M2/V1) and a metal trimer at V1 (M3/V1) respectively. (b) Detachment energies of a metal atom from a V2 (M1/V2), a metal dimer at V2 (M2/V2) and a metal trimer at V2 (M3/V2) respectively.

In experiment, metal atoms are deposited and diffuse on graphene until capture by defects. Then the subsequent deposited metal atoms can adsorb on or bind to the metal atom captured by defects. Thus the later coming metal atom can be aggregated at defects to form a stable metal dimer especially at small vacancies such as V1 and V2. While various adsorption configurations (i.e., various sizes of metal clusters on various size of vacancies) may co-exist after the initial deposition of metal atoms, our calculation results suggest that V1 and V2 vacancies with a metal dimer attached would be preferred locations for the intercalation to take place upon consequent high temperature annealing (flashing), since the detachment energy for a metal atom from the metal dimer at the V1 and V2 in graphene is smaller. We show that detachment of a metal atom from a

metal trimer at V1 and V2 in graphene is already harder than from a metal dimer. Detachment energy of a metal atom from a large metal cluster or island would approach to the energy difference between the corresponding bulk cohesive energy of the metal and the adsorption energy of the metal atom on pristine graphene (i.e., E_c-E_a), which is also larger than the detachment of metal atom from the dimer at V1 and V2 in graphene. While the present calculations are done for a free-standing graphene, we believe the conclusion can be applied to the case with graphene on a substrate if the interaction between the metal atom and the substrate is similar for the metal atom at the vacancy or away from the vacancy. Metal dimers at V1 and V2 in graphene can also be formed after each annealing cycle and serve as new precursors for next intercalation.

Finally, we note that the energetics determined in this study could key provide input to comprehensive stochastic modeling exploring the kinetics of the intercalation process [39]. Such modeling would include metal deposition, diffusion across the graphene surface to defects, aggregation at defects, detachment of metal atoms at least from dimers at defects and subsequent intercalation under the graphene sheet, and nucleation of intercalated metal nanoclusters. It is expected that higher temperatures would be required so that detachment of atoms from dimers occurs quickly before aggregation of other atoms at defects causing growth of larger clusters.

4.CONCLUSION

In order to identify which step is the determining step in the intercalation process of transition and noble metals through small vacancy defects in graphene, we investigated the adsorption and diffusion of the metal atoms on graphene by first-principles calculations. Our calculated results show that the energy barrier for a metal atom to penetrate a graphene vacancy from one side to another side is not large if the size of the vacancy is larger than a mono-vacancy. However, the intercalated Cu, Pt, Fe, Ru atoms could be easily trapped by defects and hard to proceed the

intercalation. It is interesting to note that the detachment energy for removing a metal atom from an intact metal dimer at a small vacancy defect is significantly reduced. The penetration barrier for an intact metal dimer through either a mono-vacancy or di-vacancy in graphene is also much smaller than its detachment energy from the metal dimer at defect. This result indicates the metal intercalation through graphene vacancy defects would take place through the metal dimer formation and penetration at the small (one or 2 missing atoms) vacancy defects as intermediate stage. We find the detachment energy for a metal atom from a metal dimer are the lowest, suggesting atom detachment from a metal dimer at the small vacancy defects would be very relevant events for metal intercalation in experiment. The limiting factor for the whole intercalation process is the detachment of the metal atoms from the metal dimer at the vacancy defects. This finding provides a new perspective aiding understanding and identification of the defect-assisted intercalation mechanism.

AUTHOR INFORMATION

Corresponding Author

Email: liuxj100@nenu.edu.cn

Author Contributions

Yue Liu: Methodology, Investigation, Conceptualization, Data curation, Writing- original draft. Xiaojie Liu: Conceptualization, Data curation, Validation, Resources, Writing-review&editing, Supervision. Cai-Zhuang Wang: Writing- review&editing, Supervision. Han Yong: Methodology, Writing-editing. James W. Evans: Writing-review&editing, Supervision. Ann Lii-Rosales: Methodology, Writing-editing. Michael C. Tringides: Writing -review&editing. Patricia A. Thiel: Conceptualization, Supervision.

Notes

The authors declare no competing financial interest.

ACKNOWLEDGMENT

XL and YL acknowledge the support by the National Natural Science Foundation of China under Grant No. 11574044 and the Fundamental Research Funds for the Central Universities. Work at Ames Laboratory was supported by the U.S. Department of Energy (DOE), Office of Science, Basic Energy Sciences, through the Materials Science and Engineering Division for CZW, YH, ALR, MCT, and PAT and through the Division of Chemical and Biological Sciences for JWE, including a grant of computer time at the National Energy Research Supercomputing Center (NERSC) in Berkeley. Ames Laboratory is operated for the U.S. DOE by Iowa State University under contract # DE-AC02-07CH11358.

REFERENCES

(1) Riedl, C.; Coletti, C.; Iwasaki, T.; Zakharov, A. A.; Starke, U. Quasi-free-standing epitaxial graphene on SiC obtained by hydrogen intercalation. *Phys. Rev. Lett.* **2009**, *103*, 246804.

(2) Martín-Recio, A.; Romero-Muñiz, C.; Pou, P.; Pérez, R.; Gómez-Rodríguez, J. M. Combining nitrogen substitutional defects and oxygen intercalation to control the graphene corrugation and doping level. *Carbon* **2018**, *130*, 362-368.

(3) Carnevali, V.; Patera, L. L.; Prandini, G.; Jugovac, M.; Modesti, S.; Comelli, G.; Peressi, M.; Africh, C. Doping of epitaxial graphene by direct incorporation of nickel adatoms. *Nanoscale* **2019**, *11*, 10358-10364.

(4) Anderson, N. A.; Hupalo, M.; Keavney, D.; Tringides, M.; Vaknin, D. Intercalated rare-earth metals under graphene on SiC. *J. Magn. Magn. Mater.* **2019**, *474*, 666-670.

(5) Gargiani, P.; Cuadrado, R.; Vasili, H. B.; Pruneda, M.; Valvidares, M. Graphene-based synthetic antiferromagnets and ferrimagnets. *Nat. Commun.* **2017**, *1*, 699.

(6) Li, Y.; West, D.; Huang, H.; Li, J.; Zhang, S. B.; Duan, W. Theory of the Dirac half metal and quantum anomalous Hall effect in Mn-intercalated epitaxial graphene. *Phys. Rev. B* **2015**, *92*, 201403.

(7) Krivenkov, M.; Golias, E.; Marchenko, D.; Sánchez-Barriga, J.; Bihlmayer, G.; Rader, O.; Varykhalov, A. Nanostructural origin of giant Rashba effect in intercalated graphene. *2D Mater.* **2017**, *4*, 035010.

(8) Rosenzweig, P.; Karakachian, H.; Link, S.; Küster, K.; Starke, U. Tuning the doping level of graphene in the vicinity of the Van Hove singularity via ytterbium intercalation. *Phys. Rev. B* **2019**, *100*, 035445.

(9) Sung, S.; Kim, S.; Lee, P.; Kim, J.; Ryu, M.; Park, H.; Kim, K.; Min, B. I.; Chung, J. Observation of variable hybridized-band gaps in Eu-intercalated graphene. *Nanotechnology* **2017**, *28*, 205201.

(10) Kim, M.; Tringides, M. C.; Hershberger, M. T.; Chen, S.; Hupalo, M.; Thiel, P. A.; Wang, C. Z.; Ho, K. M. Manipulation of Dirac cones in intercalated epitaxial graphene. *Carbon* **2017**, *123*, 93.

(11) Minato, T.; Abe, T. Surface and interface sciences of Li-ion batteries-research progress in electrode-electrolyte interface. *Prog. Surf. Sci.* **2017**, *92*, 240-280.

(12) Weller, T. E.; Ellerby, M.; Saxena, S. S.; Smith, R. P.; Skipper, N. T. Superconductivity in the intercalated graphite compounds C6Yb and C6Ca. *Nat. Phys.* **2015**, *1* (1), 39.

(13) Watcharinyanon, S.; Johansson, L. I.; Xia, C.; Flege, J. I.; Meyer, A.; Falta, J.; Virojanadara, C. Ytterbium intercalation of epitaxial graphene grown on Si-face SiC. *Graphene* **2013**, *2*, 66-73.

(14) Cui, Y.; Gao, J.; Jin, L.; Zhao, J.; Tan, D.; Fu, Q.; Bao, X. An exchange intercalation mechanism for the formation of a two-dimensional Si structure underneath graphene. *Nano Research.* **2012**, *5* (5), 352-360.

(15) Daukiya, L.; Nair, M. N.; Hajjar-Garreau, S.; Vonau, F.; Aubel, D.; Bubendorffff, J. L.; Cranney, M.; Denys, E.; Florentin, A.; Reiter, G.; et al. Highly n-doped graphene generated through intercalated terbium atoms. *Phys. Rev. B* **2018**, *97*, 035309.

(16) Lii-Rosales, A.; Han, Y.; Yu, K. M.; Jing, D.; Anderson, N.; Vaknin, D.; Tringides, M. C.; Evans, J. W.; Altman, M. S.; Thiel, P. A. Reverse-engineering of graphene on metal surfaces: a case study of embedded ruthenium. *Nanotechnology* **2018**, *29*, 505601.

(17) Lii-Rosales, A.; Han, Y.; Evans, J. W.; Jing, D.; Zhou, Y.; Tringides, M. C.; Kim, M.; Wang, C. Z.; Thiel, P. A. Formation of multilayer Cu islands embedded beneath the surface of graphite: characterization and fundamental insights. *J. Phys. Chem. C* **2018**, *122*, 4454-4469.

(18) Zhou, Y.; Lii-Rosales, A.; Kim, M.; Wallingford, M.; Jing, D.; Tringides, M. C.; Wang, C. Z.; Thiel, P. A. Defect-mediated, thermally-activated encapsulation of metals at the surface of graphite. *Carbon* **2018**, *127*, 305-311.

(19) Lii-Rosales, A.; Han, Y.; Lai, K. C.; Jing, D.; Tringides, M. C.; Evans, J. W.; Thiel, P. A. Fabricating Fe nanocrystals via encapsulation at the graphite surface. *J. Vac. Sci. Technol. A* **2019**, *37* (6), 061403.

(20) Lii-Rosales, A.; Han, Y.; Julien, S. E.; Pierre-Louis, O.; Jing, D.; Wan, K. T.; Tringides, M. C.; Evans, J. W.; Thiel, P. A. Shapes of Fe nanocrystals encapsulated at the graphite surface. *New J. Phys.* **2020**, *22* (2), 023016.

(21) Lii-Rosales, A.; Han, Y.; Jing, D.; Tringides, M. C.; Thiel, P. A. Search for encapsulation of platinum, silver, and gold at the surface of graphite. *Phys. Rev. Research* **2020**, *2* (3), 033175.

(22) Yu, L.; Du, C.; Liu, X. Dy adsorption and penetration on defected graphene by first-principles calculations. *Mater. Res. Express* **2018**, *5*, 025022.

(23) Lu, X.; Liu, Y.; Shao, M.; Liu, X. Defect-mediated intercalation of dysprosium on buffer layer graphene supported by SiC (0001) substrate. *Chem. Phys. Lett.* **2020**, *742*, 137162.

(24) Jin, L.; Fu, Q.; Yang, Y.; Bao, X. A comparative study of intercalation mechanism at graphene/Ru (0001) interface. *Surf. Sci.* **2013**, *617*, 81-86.

(25) Han, Y.; Lii-Rosales, A.; Tringides, M. C.; Evans, J. W.; Thiel, P. A. Energetics of Cu adsorption and intercalation at graphite step edges. *Phys. Rev. B* **2019**, *99*, 115415.

(26) Liu, L.; Du, C.; Wang, S.; Chen, S. Three new bifunctional additives for safer nickel-cobalt-aluminum based lithium ion batteries. *Chin. Chem. Lett.* **2018**, *29*, 1781-1784.

(27) Noor-A-Alam, M.; Hamid, U.; Shin, Y. H. Switchable polarization in Mn embedded graphene. *Sci. Rep.* **2018**, *8*, 4538.

(28) Zhang, Y.; Zhang, H.; Cai, Y.; Song, J.; He, P. The investigation of cobalt intercalation underneath epitaxial graphene on 6H-SiC (0001). *Nanotechnology* **2017**, *28*, 075701.

(29) Kresse, G.; Furthmuller, J. Efficiency of ab-initio total energy calculations for metals and semiconductors using a plane-wave basis set. *Comput. Mater. Sci.* **1996**, *6* (1), 15-50.

(30) Kresse, G.; Joubert, D. From ultrasoft pseudopotentials to the projector augmented-wave method. *Phys. Rev. B* **1999**, *59* (3), 1758-1775.

(31) Blöchl, P. E. Projector augmented-rave method. *Phys. Rev. B* **1994**, *50* (24), 17953-17979.

(32) Perdew, J. P.; Wang, Y. Accnrate and simple analytic representation of the electron-gas correlation energy. *Phys. Rev. B* **1992**, *45* (23), 13244-13249.

(33) Perdew, J. P.; Burke, K.; Ernzerhof, M. Generalized gradient approximation made simple. *Phys. Rev. Lett.* **1996**, *77* (18), 3865-3868.

(34) Henkelman, G.; Jónsson, H. Improved tangent estimate in the nudged elastic band method for finding minimum energy paths and saddle points. *J. Chem. Phys.* **2000**, *113*, 9978-9985.

(35) Liu, X.; Wang, C. Z.; Hupalo, M.; Lin, H. Q.; Ho, K. M.; Tringides, M. C. Metals on graphene: interactions, growth morphology, and thermal stability. *Crystals* **2013**, *3*, 79-111.

(36) Engstfeld, A. K.; Hoster, H. E.; Behm, R. J.; Roelofs, L. D.; Liu, X.; Wang, C. Z.; Han, Y.; Evans, J. W. Directed assembly of Ru nanoclusters on Ru (0001)-supported graphene: STM studies and atomistic modeling. *Phys. Rev. B* **2012**, *86*, 085442.

(37) Julien, S. E.; Lii-Rosales, A.; Wan, K. T.; Han, Y.; Tringides, M. C; Evans, J. W.; Thiel, P. A. Squeezed nanocrystals: equilibrium configuration of metal clusters embedded beneath the surface of a layered material. *Nanoscale* **2019**, *11*, 6445-6452.

(38) Li, W.; Huang, L.; Tringides, M. C.; Evans, J. W.; Han, Y. Thermodynamic preference for atom adsorption on versus intercalation into multilayer graphene. *J. Phys. Chem. Lett.* **2020**, *11*, 9725-9730.

(39) Han, Y.; Lii-Rosales, A.; Tringides, M. C.; Evans, J. W. Competitive formation of intercalated versus supported metal nanoclusters during deposition on layered materials with surface point defects. *J. Chem. Phys.* **2021**, *154* (2), 024703.

TOC Graphic:

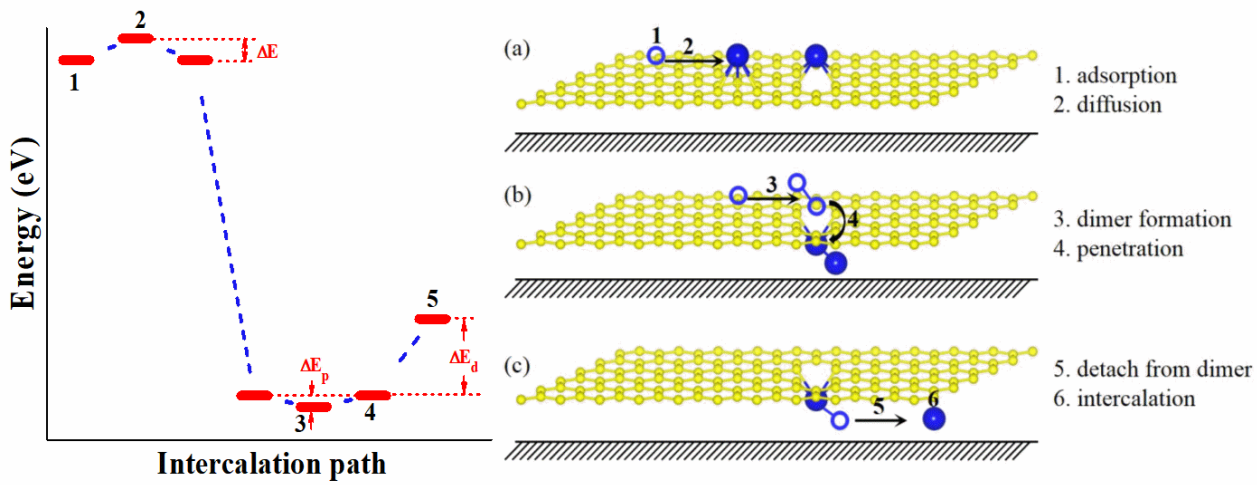
Energy (eV)
Intercalation path
1
2
3
4
5
ΔE
ΔE_p
ΔE_d
(a)
(b)
(c)
6
1. adsorption
2. diffusion
3. dimer formation
4. penetration
5. detach from dimer
6. intercalation